J. Fluid Mech. (1983), *vol.* 129, *pp.* 365–383
Printed in Great Britain

Experiments on solitary internal Kelvin waves

By T. MAXWORTHY

Departments of Mechanical and Aerospace Engineering, University of Southern California, Los Angeles, CA 90089-1453

(Received 23 December 1981 and in revised form 18 June 1982)

Elementary calculations indicate that the effect of the Earth's rotation is likely to be important in the dynamics of most internal waves in oceans, lakes and the atmosphere. Here we present measurements of the structure and properties of one class of such waves, namely solitary internal Kelvin waves, in which the Coriolis force generated by wave motion in a stratified fluid is opposed by a pressure gradient and hence change in wave amplitude along its crest. We confirm that the wave speed is independent of the rate at which the system rotates and depends only on the stratification and maximum wave amplitude. However, rotation is shown to have a large effect on both the rate at which the amplitude varies with time and the 'cross-stream' structure of the wave. In accordance with well-established theory, the amplitude transverse to the direction of propagation varies exponentially. This results in a decreasing wave speed with increasing distance from the wall, which in turn requires the wave front be curved backwards in order for the wave as a whole to propagate at a speed given by its maximum amplitude. Such a front curvature is not contained within the available theories. The rapid decay of wave amplitude is found to be due to the generation of inertial waves in the homogeneous fluid above and below the internal wave, and a reasonably successful scaling of this effect has been found. We also discuss the adjustment of the waves to geostropic balance and comment on applications of our results to natural systems.

1. Introduction

Here we present a relatively straightforward extension of some recent work on the generation of internal solitary waves by the collapse of a mixed region into a stably stratified fluid (Maxworthy 1980, hereinafter referred to as M; Amen & Maxworthy 1980). By placing a shortened version of the wave tank used in those studies onto a rotating table, we have studied the generation and unique properties of large-amplitude solitary internal Kelvin waves. To our knowledge such waves have not been studied quantitatively before in the laboratory, although Suberville (1974) has studied sloshing in a rotating, stratified tank and has produced a moving-picture film of solitary, Kelvin waves; while related work on gravity currents in a rotating tank has recently been reported (Stern, Whitehead & Hua 1982; R. W. Griffiths private communication). It is also clear that the results to be presented should have a considerable influence on our interpretation of a number of experiments in natural systems where the relevant parameters are within the range of our laboratory experiments. The most important of the latter is the internal Rossby radius of deformation ($L = Nd/f$ as usually defined; where N is the intrinsic frequency $[-(g/\rho)\,\partial\rho/\partial z]^{\frac{1}{2}}$, d a depthscale, ρ the density, g the gravitational acceleration, z the vertical coordinate and f twice the local rotation rate (Ω/s)). In cases where N and/or d are rapidly changing functions of depth it is necessary to substitute $L_c = c/f$, where

c is the wave speed of the appropriate internal wave mode, to retain the original physical concept of L, which is to compare a typical long-wave speed to the rate of rotation of the system. We can therefore discuss waves in nature and waves in our laboratory tank by comparing this length to an intrinsic length in the problem, e.g. the channel width W, in both the field and experiment. Several cases come to mind. In the studies of Mortimer (1955), Thorpe (1971) and Thorpe, Hall & Crofts (1972) of large-amplitude waves and bores in Loch Ness (see Thorpe 1974) the measured wave speed was about 37 cm/s, resulting in a value of $L_c \approx 3.3$ km, which we note is about twice the width of the Loch. In this case Mortimer (1955) suggested a sequence of isotherm shapes that qualitatively conformed to those one would expect of internal seiches modified by the effects of rotation. More recently Hamblin (1978) has calculated these effects in more detail for Kamloops Lake, and finds moderately good agreement with observations. In the measurements of Smith & Farmer (1977) and Farmer & Smith (1980) on internal waves in Knight Inlet B.C. they found a wave speed of around 50 cm/s, corresponding to a value of $L_c \approx 4.5$ km, about one and a half times the width of the channel. Farmer (1978) suggested that serious consideration should be given to rotational effects, since L_c (2–3 km) in his case was much smaller than the width (2–10 km) of Babine Lake in which he conducted his study. Hunkins & Fliegel (1978) measured wave speeds of 35–40 cm/s, corresponding to $L_c = 3.6$–4.2 km in a lake of width of approximately 5 km. Finally, in atmospheric flows theories of both the Southerly Buster (Baines 1980; Gauntlett 1981) and the waves propagating around the tip of South Africa (Anh & Gill 1981; Bannon 1981), invoke internal Kelvin waves as a plausible explanation, and such waves appear to have much in common with those to be described.

The linear theory of internal Kelvin waves is well established (e.g. Pedlosky 1979), while the weakly nonlinear theory has recently been calculated by L. G. Redekopp (Private communication). For the moment we note that such waves have amplitudes which vary exponentially along the wave crest and have no transverse velocity. The pressure difference thus generated is supported by the wall along which the wave propagates.

2. Apparatus

A section of rectangular Plexiglas channel 360 cm long × 20 cm wide × 30 cm high was mounted on an existing rotating table (figure 1). Before rotation the lower 15 cm was filled with a salt solution of known density ($\rho_1 = 1.04$ or 1.08 g/cm^3). The table was then set into rotation at a known rate, and the tank was filled slowly, through a floating diffuser, with fresh water of density $\rho_2 = 1.00$ g/cm^3. The float and supply tube were then removed. Usually the interface produced between the two constant-density layers was too thin for our purposes, and a wire mesh had to be drawn through the interface several times in order to thicken it. After one hour, when diffusion had smoothed out all irregularities, two layers of dyed freon–kerosene droplets were introduced to settle at two known levels. The required drop densities were found by noting that the density profile was closely represented by

$$\rho(\eta) = \bar{\rho}\,[1 - \tilde{\omega}\tanh\alpha\eta]$$

(see Benjamin 1967; Faust 1981; M), where η is the height from the midplane of the interface, $\bar{\rho}$ is the mean density $\frac{1}{2}(\rho_1+\rho_2)$, $\tilde{\omega}$ is a measure of the density difference and equals $(\rho_2-\rho_1)/(\rho_2+\rho_1)$, and α is the inverse scale height of the density distribution. The drop densities were calculated so that they were in equilibrium at heights $1/\alpha$

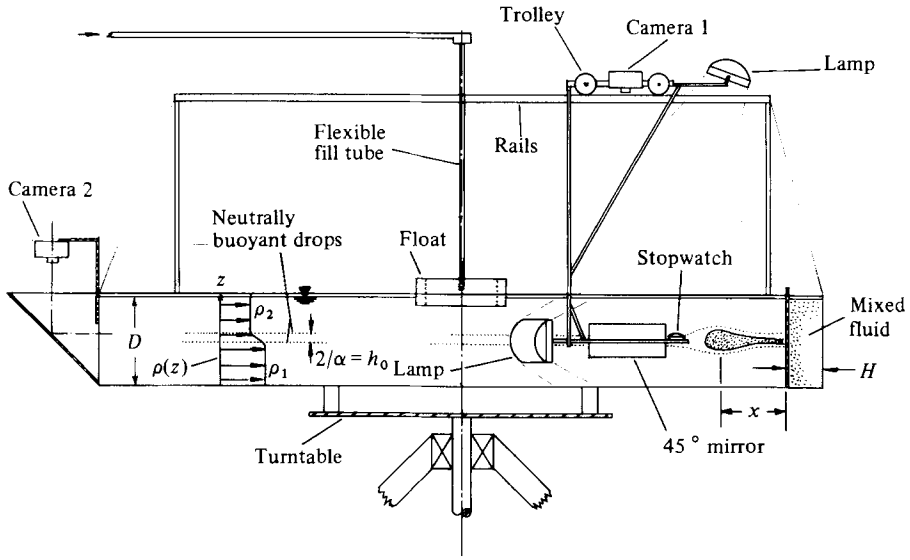

FIGURE 1. Apparatus. We attempt to show all of the experimental apparatus and procedure on one drawing. The fill tube and float were removed before the experiment started. The barrier, shown in place here, was removed to create the initial internal gravity current, which is shown.

from the midlevel (i.e. at levels at which $\alpha\eta = 1$ and $\tanh\alpha\eta = 0.762$). Thus the distance between the layers was equal to $2/\alpha \equiv h_0$, while the distortions of the layers, as the waves propagated, were a convenient and consistent measure of the wave amplitude, which could then be related to the theoretical developments of Benjamin (1967) and Joseph (1977), for example.

The wave themselves were produced as in M by trapping fluid behind a barrier (see figure 1) and then mixing it up completely. Upon pulling out the barrier and coincidentally starting a stopwatch in the field of view of a recording camera, the mixed fluid collapsed along the midplane of the interface generating a series of solitary Kelvin waves as it did so.

Because of their three-dimensional structure, these waves had to be viewed from three mutually orthogonal directions. A motorized camera was mounted on a carriage above the tank, from which it could view the plan view of the wave and, reflected in a mirror, a side view. A second camera was mounted at the end of the tank so that we could photograph a front view of the wave as it approached the endwall of the tank. It was clearly difficult to take such front-view photographs at intermediate locations; however, this loss of information was not serious once the basic structure of the waves had been inferred from the information that was available.

A large number of experiments were performed covering, in particular, a large range in Ω from 0.0164/s to 0.262/s with intermediate values of 0.0330/s, 0.0650/s and 0.133/s. Two density differences $\rho_2 - \rho_1$ were used: 0.04 g/cm^3 and 0.08 g/cm^3, although the majority of the experiments were performed with the former value. Three values of mixed-region width H were considered: 0.64, 1.91 and 3.18 cm. Under less-precise control were the values of h_0. We attempted to use two basic values, 1.5 and 2.5 cm, but the range finally stretched in irregular intervals from 1.3 to 2.5 cm. Ultimately a total of 41 experiments were performed and analysed.

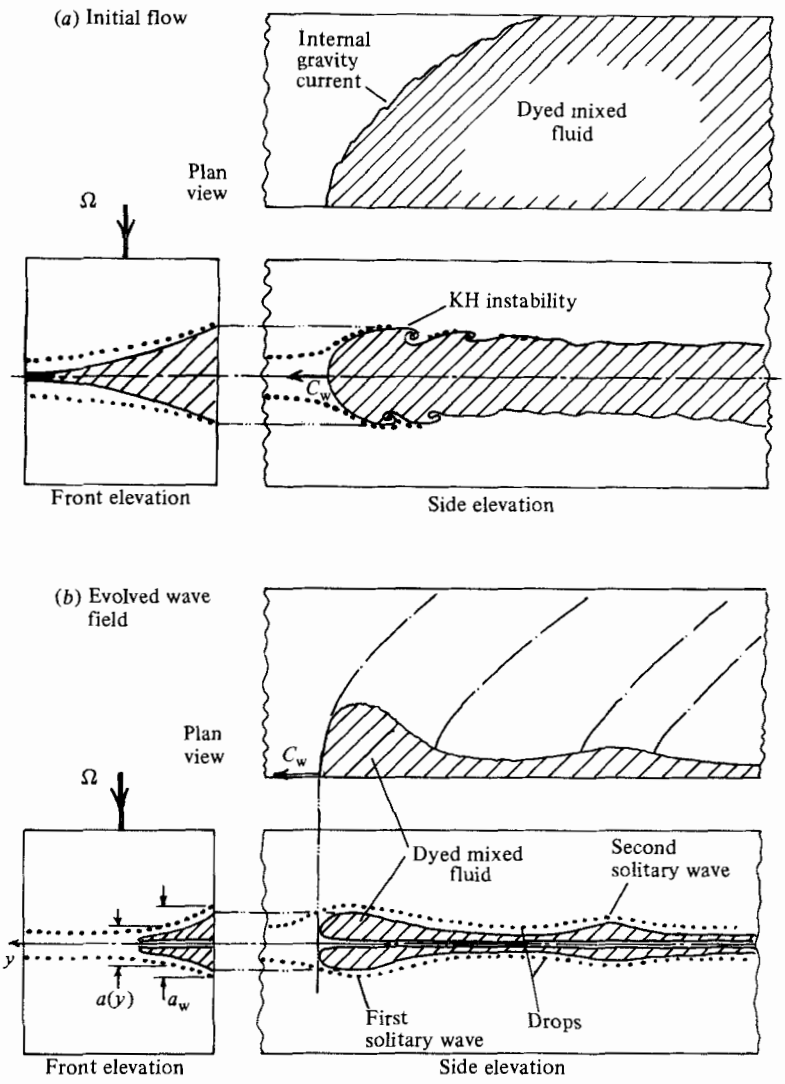

FIGURE 2. (*a*) Initial form taken by the internal gravity current shortly after barrier removal. Three views are shown to indicate the wedge-shaped three-dimensional nature of this feature. For large amplitudes, i.e. large H/h_0, the front was turbulent with a Kelvin–Helmholtz (K-H) type of shear-flow instability very evident. (*b*) Evolved wave field. The state shown in (*a*) has evolved into a sequence of solitary waves, two of which are drawn here. The wave amplitude decreases away from the left-hand wall and 'closed streamlines' only existed part of the way across the tank.

3. Results

3.1. *Preliminary, qualitative observations*

As a first step we believe it is useful to consider a typical wave evolution so that the quantitative results can be presented in a logical way later. On the one hand, we know that the prior results of M must be approached as $\Omega \to 0$, although it turns out that even a very small rotation rate, for which $L_c \gg W$, showed measurable deviations from the previous results. As a result it is helpful to consider initially the other limit for which $L_c \lesssim W$ and for which the effects of rotation are most dramatic.

Under such circumstances the removal of the barrier created an internal gravity current, which because of the clockwise rotation started to move along the left-hand wall of the tank (looking in the direction of motion). This mass of constant-density fluid distorted the isopycnal surfaces symmetrically about the midplane of the interface; however, the thickness of the region of mixed fluid varied across the channel (figures 2*a*, 3*a*). Significantly the wave front when viewed from above was inclined backwards, while the side view was indistinguishable from the waveforms found in M. As the forward wave evolved further more waves began to emerge behind it, although the tank was too short to allow their full evolution, as in M. However, by the time the wave had almost reached the end of the tank it had the form shown in figures 2(*b*) and 3(*a*). A compact blob of mixed fluid was being carried along by the wave. As in M, as the wave amplitude decreased, owing to internal dissipation, the mixed fluid slowly leaked from the rear of the wave until eventually no closed stream surfaces could exist and the wave left the mixed fluid behind completely. In figure 2(*b*) we have also tried to indicate, by the chain-dotted lines, that the lines of constant phase across the wave were curved backwards as indicated by the distortion of the sheet of marker drops. This curvature has no equivalent in the theory of linear Kelvin waves since it is a reflection of nonlinear effects – in particular, the dependence of wave speed upon wave amplitude. In the simplest case this can be expressed as $C = C_0(1+ka)$ (see Benjamin 1967), where C_0 is the linear long-wave speed, a (see figure 2) the wave amplitude and K a calculable constant. In our case, since a decreased away from the wall the wave speed must also decrease and the wave front must be curved in order for the whole to propagate at its maximum velocity, that determined by the amplitude at the wall (see figure 4).

In cases where L was larger than in the one described above, the region of closed streamlines could extend completely across the tank (figure 3*b*). Even for the lowest rotation rate possible in the present equipment (for which $L_c \approx 210$ cm, i.e. 10 times the tank width), the wave front was still noticeably curved (figure 3*b*) owing to the small change in wave speed across the wave and the cosinusoidal dependence on wave angle (figure 4), which is also weak as $\theta \to 90°$. It is also of interest that no reflected waves were observed owing to the interaction of the curved wave front with the sidewall of the channel. In all the experiments several distinct solitary waves were formed, typically 3 or 4; however, the tank was too short to allow the complete evolution of the full complement of waves, although we suspect that, as in M, more were formed when the volume of the mixed region was larger.

The other interesting qualitative observation, which has not yet been fully explored, concerns the wave interaction with the endwall. Here, when L_c was small, the compact blob travelling along the one wall turned the two corners at the end of the tank and proceeded along the opposite long wall, with, however, a much-diminished amplitude due to substantial turbulence generation at the sharp corners. When L_c was large, the interaction still created a large variation in amplitude across the wave during the initial part of the interaction, even when it was barely apparent in the oncoming wave before interaction. We presume this was due to the relatively large wave curvature that existed, even in this case, so that the forward part of the wave interacted with the wall before the trailing part. This large disturbance then travelled across the endwall of the tank and then back along the other sidewall, creating a number of smaller waves as it did so.

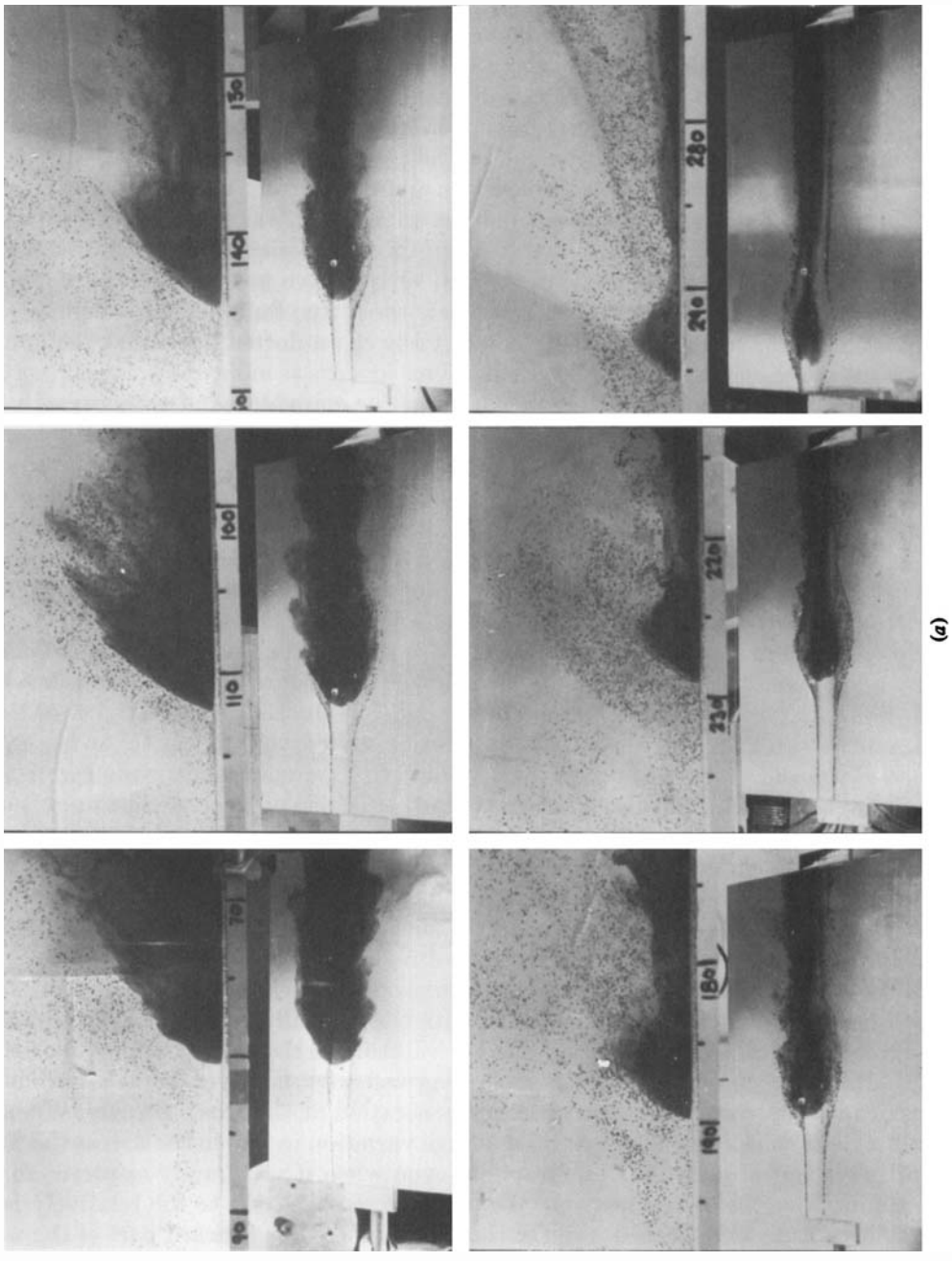

(a)

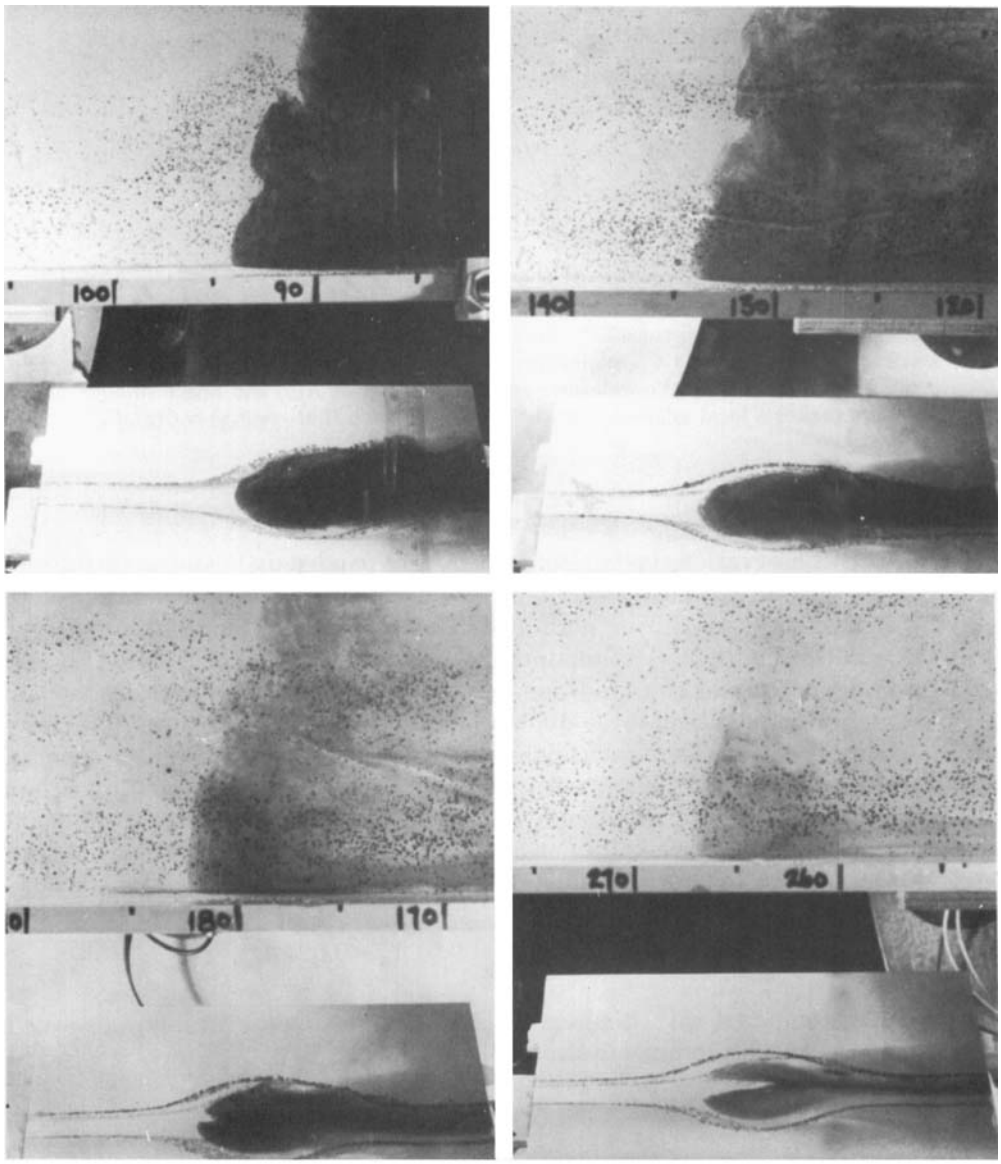

(*b*)

FIGURE 3. Sequence of photographs of the plan and side views of the waves for two extreme cases. (*a*) A small value of $L_c = 9$ cm showing the large wave-front curvature and the identity of the side view with that found in M. (*b*) A large value of $L_c = 192$ cm. Despite the fact that L_c is some ten times the channel width, wave-front curvature is still quite noticeable (cf. figure 10).

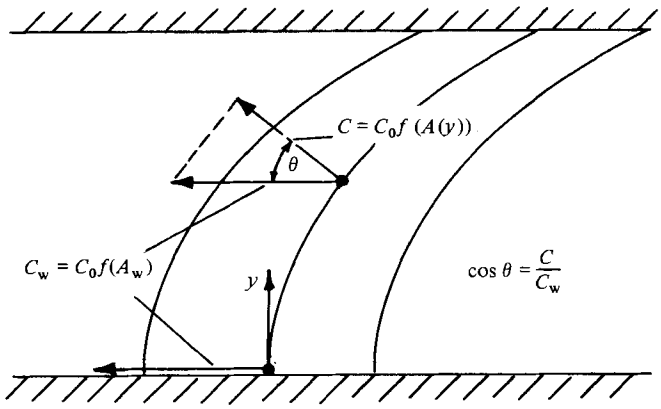

FIGURE 4. Curved shape of the constant-phase lines of a propagating solitary Kelvin wave. The whole wave moves at a velocity C_w set by the maximum wave amplitude A_w at the wall. Those parts of the wave further from the wall have smaller amplitudes $A(y)$ and hence smaller velocity $C(y)$. The wave makes a local angle $\theta(y)$ to the horizontal such that $\cos\theta(y) = C(y)/C_w$.

3.2. *Quantitative observations*

The qualitative observations just presented can be expanded upon and quantitatively evaluated in several instances. We start by discussing the overall motion of the evolving first wave by measuring both its displacement x and the total wave height a_w at the wall (see figure 2) as a function of time t. A truly typical x versus t history is shown in figure 5(*a*) for the conditions shown on that graph. By taking the local slope through four points at three different locations along this curve, local wave speeds C_w were measured. The dimensionless amplitudes $A_w = a_w/h_0 - 1$ corresponding to the locations at which C_w was measured are also indicated on figure 5(*a*). C_w was then made dimensionless by dividing by $[gh_0(\rho_2-\rho_1)/\bar{\rho}]^{\frac{1}{2}}$. Approximately 100 points representing the dependence of dimensionless wave speed on dimensionless wave amplitude are shown in figure 5(*b*). These points are well represented by the curve

$$\frac{C_w}{(g'h_0)^{\frac{1}{2}}} = \{0.33 \pm 0.02\}\{1 + 0.51A_w - 0.024A_w^2\},$$

which is to be compared with Benjamin's (1967) expression for an internal wave in an infinitely deep fluid; in our notation

$$\frac{C_w}{(g'h_0)^{\frac{1}{2}}} = 0.35\{1 + 0.3A_w\},$$

Curves representing both of these expressions are drawn on figure 5(*b*). We note especially that no dependence on L_c can be distinguished, even though it varied by a factor of 20 over the whole range of the experiments. This is exactly what one would expect from the theory of Kelvin waves, since in that case only the transverse wave structure is affected by the overall rotation of the wave guide.

In this figure we also show that for low amplitudes the difference between our results and those of Benjamin (1967) can be explained to some extent by the finite depth D of our waveguide. Using Joseph (1977) we can correct Benjamin's infinite-depth result and also show this on figure 5(*b*) for a depth ratio D/h_0 of 15, typical of our experimental range. It is also possible that some of the small scatter of figure

5(*b*) is due to the different values of D/h_0 used, but no consistent trend with this parameter can be determined from the data.

At large values of A_w the width of the propagating mixed region of fluid and the distance between the two lines of particles were the same. One might anticipate that under these circumstances the motion would approximate that due to a gravity current, so that the effects of the distribution of stratification would be small. On figure 5(*b*) we have drawn a line which represents the velocity of propagation of a gravity current with the same amplitude as the waves observed in the present case from the curve presented in Britter & Simpson (1978) for the case of a 'slip' boundary condition. The basis for the calculation is as follows. The velocity of propagation of a gravity current is given by

$$U = f(\phi)\left(g\frac{\Delta\rho}{\rho}h_4\right)^{\frac{1}{2}},$$

where $\Delta\rho$ is the density difference between the current and its surroundings, h_4 is the height of the fluid layer behind the head of the current (see Britter & Simpson 1978) and $f(\phi)$ represents a correction due to the finite depth of the tank in which it propagates, where $\phi = h_4/\text{total depth}$. In our case $\Delta\rho = (\rho_1-\rho_2)/\rho$, $h_4 = \frac{1}{2}a_w$ and $\phi = a_w/D$.

The equation for U can now be rewritten as

$$\frac{U}{(g'h_0)^{\frac{1}{2}}} = f(\phi)\left[\frac{A_w+1}{4}\right]^{\frac{1}{2}}.$$

The curve shown in figure 5(*b*) is the above expression calculated for a representative value of $h_0 = 1.6$ cm. We see that our waves are approaching this gravity-current limit, although we have too few points to be sure of the precise asymptote.† On this same figure we also show a few points from a recent study by Faust (1981) of large-amplitude non-rotating density fronts between two layers of constant density for which H was very large. Only in a few cases did identifiable waves appear, but his front velocity and our wave velocity appear to overlap consistently for parameter values which are comparable. Both this work and our own are clearly related to a more recent paper of Britter & Simpson (1981) in which they discuss the connections between gravity currents on interfaces, as studied here, and those with slip and no-slip boundary conditions at a solid surface. At the suggestion of a referee, on figure 5(*b*) we also plot results from this paper for values of $A_w \geqslant 4$ from their figure 5: our results and theirs are seen to be in reasonable agreement in this limit.

While analysing the measurements discussed above, it became clear that the effect of tank rotation on the decay rate of wave amplitude was very strong. The data set was expanded to include the measurement of wave amplitude from every photograph. With some exceptions, the amplitude varied as

$$\frac{A_w(t)}{A_w(0)} = \mathrm{e}^{-(t-t_0)/\sigma},$$

where t is the time and t_0 the time for the first observation of amplitude $A_w(0)$.

† In our case the interface between the mixed fluid and the surroundings is thicker than that in the conventional gravity-current situation because of the presence of the initial density distribution. This in turn results in a more-stable interface, so that the height of the head (h_3+h_4, in the Britter–Simpson notation) is approximately equal to h_4. It is likely that some of the differences between the present experiments at large values of A_w and the gravity-current results of Britter & Simpson (1978) are due to the inaccuracy of this assumption.

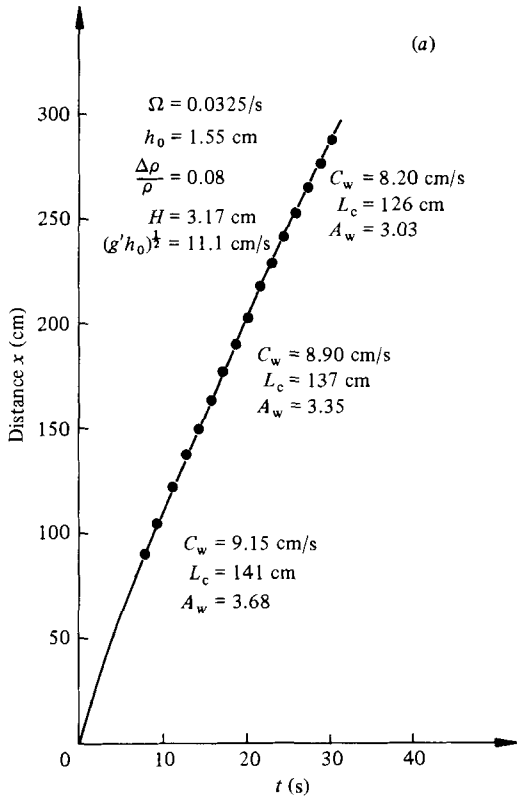

FIGURE 5(*a*). For caption see facing page.

Figure 6 shows two such curves for identical initial conditions, except that L_c is 137 cm in one case and 32 cm in the other. This demonstrates the dramatic effect that increasing the rotation rate has on increasing the internal wave dissipation. The reason for the majority of this increase is clear. The propagating internal wave appears as a moving topographical disturbance to the homogeneous fluid above and below the wave guide. It can generate inertial waves in a manner entirely equivalent to that observed by Heikes & Maxworthy (1982) above a solid object being towed through a rotating, unstratified medium.† In figure 7 we show a computer simulation of these waves, using the method outlined in this reference, for a set of conditions typical of oceanic internal waves and essentially assuming that the disturbance due to the wave can be replaced by an equivalent solid body. Similar waves can be seen in the present experiments, but the photographs are not suitable for reproduction here. The effect of these inertial waves is to cause a wave drag upon the internal wave which then results in a loss of energy from the latter. Observations show that the wave speed does not change very much during this process (typically 20%) and so we can make the following estimate of the wave-amplitude change. The rate of change of wave energy must equal the wave drag times the wave speed. Wave energy and

† I am especially grateful for discussions with Dr R. W. Griffiths and Prof. E. J. Hopfinger on their work on gravity currents in a rotating fluid which first brought the possibility of inertial wave drag to my attention.

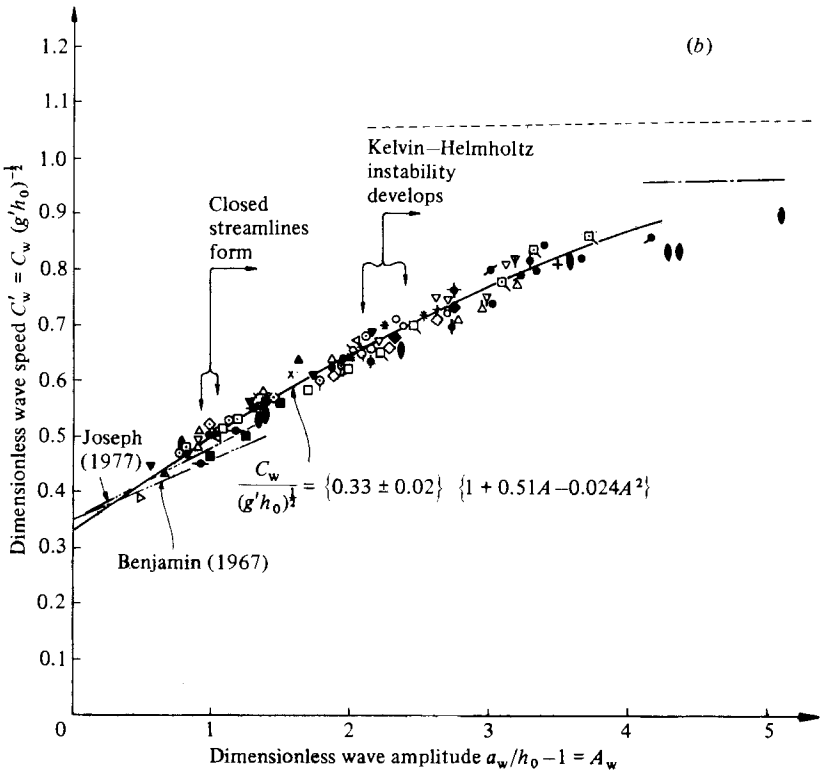

FIGURE 5. (*a*) Typical wave history, displacement x versus time t. Local values of wave velocity C_w, amplitude A_w and Rossby radius L_c are shown. (*b*) Non-dimensional local wave velocity $C_w/(g'h_0)^{\frac{1}{2}}$ versus non-dimensional wave amplitude $A_w = a_w/h_0 - 1$. These results represent values taken over a 20-fold range of L; no dependence on this parameter can be distinguished. —●—, from Faust (1981). Gravity-current data from Britter & Simpson (1978, ----; 1981, –·–·–); Benjamin (1967), —·—. $C_w = 0.35(1+0.3A_w)$; Joseph (1977), —···—. $C_w = 0.35(1+0.3A_w\,(1+h_0/D)$.

wave drag are both proportional to the square of the wave amplitude (Mason & Sykes 1983) so that we can write

$$\frac{\mathrm{d}a^2}{\mathrm{d}t} \sim \frac{\Omega \bar{c}^2 W a^2}{g'\lambda} \sim \frac{\bar{c}^3 W}{L_c g'\lambda} a^2$$

where $\bar{c}$ is the average wave speed during the period of observation. Thus $a \sim \exp\{\bar{c}^2 Wt/L_c g'\lambda\}$ for a two-dimensional wave of wavelength λ and width W. Unfortunately λ is not a clear-cut quantity in the present case owing to the variations in wave shape encountered. We therefore attempted to reduce our raw data by rescaling σ with $L_c g'/\bar{c}^3 W$. The results showed a continuing dependence on both L_c and the initial wave amplitude A_0. Presumably this was due to three effects. First, the wave is not equivalent to a two-dimensional obstacle of width W because of the large variations of wave amplitude and orientation across the tank. Secondly, the effects of variable wave shape means that the constant of proportionality in the wave-drag equation is not constant, while the ignored variation in λ must, in some way, depend on the wave amplitude. Empirically, we attempted to reduce the variations in our scaled σ by multiplying by various combinations of L_c^n and A_0^m until a satisfactory result was obtained. This is shown in figure 8, where we plot $\sigma c^3/L_c^{0.4} g' A_0$

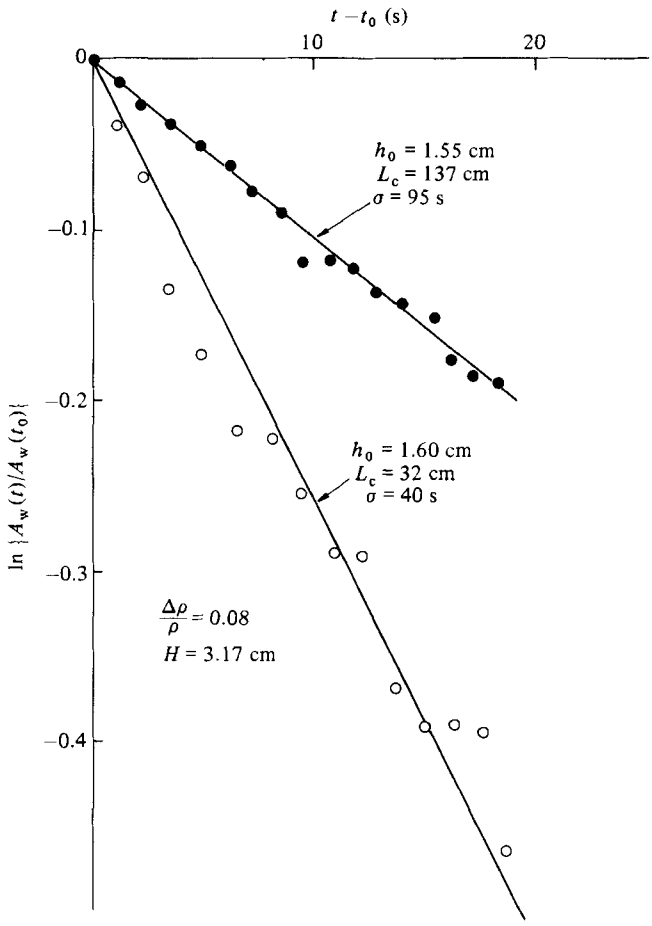

FIGURE 6. Two typical wave-amplitude decay curves for identical initial conditions, except that L_c is 137 cm for one case and 32 cm for the other.

versus L_c. The former is constant at a value of $25 \pm 20\%$ over a 20-fold change in L_c. Such an observation has interesting implications for waves in natural systems, where, as we have indicated, rotation can be expected to have a substantial effect. This change in amplitude and corresponding small change in wave speed also resulted in a change in L_c as the wave propagated and a corresponding change in the wave curvature mentioned in §3.1 and presented in more detail at the end of this section. The wave adjusted to its changing amplitude since this was taking place relatively slowly, as has also been found in other studies of solitary waves in dissipative systems (e.g. Weidman & Maxworthy 1978).

By photographing the wave as it approached the endwall of the tank we have been able to determine the cross-stream exponentially varying structure of these waves to a relatively low accuracy. Figure 8 shows measurements of the Rossby radius L_M determined from these photographs as the transverse distance from the wall at which the wave amplitude $A(y)$ is 1/e of the wall value. Again the accuracy is not high, but shows quite clearly and unexpectedly that the measured value L_M and the calculated value L_c of the Rossby radius differ by a factor of at least two. The validity of this observation is reinforced in our final quantitative results in which we calculate

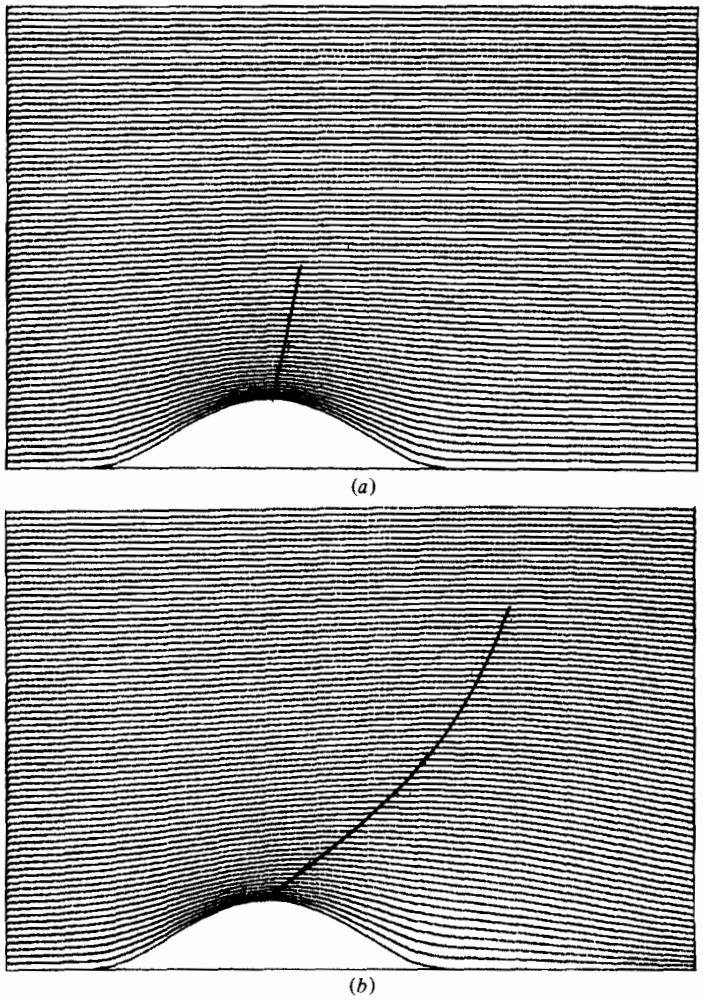

FIGURE 7. Computer simulation of the inertial wave field over a solid body with the shape of a solitary wave, calculated using the method of Heikes & Maxworthy (1982). The parameters used are typical of oceanic values, e.g. a Rossby number based on wave width of (*a*) unity, and (*b*) 0.5, and a depth ratio, i.e. wave height to fluid depth, of 0.13. The inclined lines indicate the location of the maximum displacement of each streamline. Calculations are due to Dr K. Heikes.

the shape of the wave front based on rather elementary, but nonetheless satisfying, considerations.

In figure 4 we have already explained the basis for this calculation. We assume that the velocity C_w of the wave is determined by its amplitude A_w at the wall. Owing to the decrease in wave speed with amplitude those portions of the wave farther from the wall have a lower wave speed. We make use of our experimentally determined values of both velocity (figure 5*b*) and Rossby radius (figure 9) to determine the local wave angle θ as shown in figure 4. Here then

$$\cos\theta(y) = \frac{1+0.51A_w\,e^{-2y/L_c}-0.024A_w^2\,e^{-4y^2/L_c^2}}{1+0.51A_w-0.024A_w^2},$$

where we have used the observation that $L_M \approx \frac{1}{2}L_c$. Clearly, at $y = 0$, $\theta = 0°$, and we

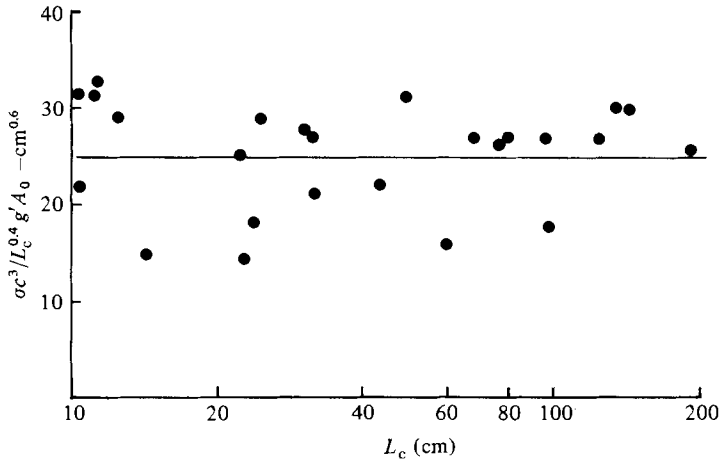

FIGURE 8. Decay rate of internal Kelvin wave versus a measure of the rotation rate of the system.

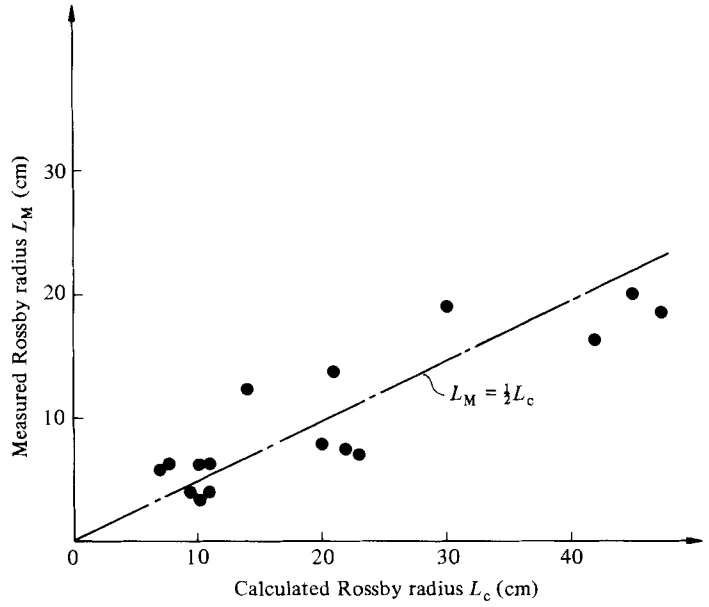

FIGURE 9. Rossby radius of deformation L_M measured from photographs of the transverse wave shape versus values L_c calculated from $C_w/2\Omega$.

can use a trivial 'shooting' technique to obtain the wave shape, knowing the value of θ at each point. The final comparison is then shown in figure 9, where the agreement between the observed and calculated fronts is seen to be quite satisfactory.

4. Conclusions and discussion

The results presented in §3 are self-explanatory to a large extent. The majority of these could have been anticipated from the prior theoretical work, namely the independence of wave speed on rotation rate, its sole dependence on stratification and

wave amplitude, and the exponential form of the cross-stream wave structure. However, these in combination have the effect of producing a wave front which is curved downstream. This effect is not contained in the available theories nor was it anticipated prior to the performance of the experiments. Also of interest was the large increase in wave-energy dissipation for small values of L_c due to inertial wave generation, even in cases where the flow was not turbulent.

In § 1 we mentioned several field studies in which internal surges and finite-amplitude waves had been studied in long thin lakes or fjords. Only Mortimer (1955) and Hamblin (1978) mention any observed effects of rotation; cross-channel variation in amplitude, in the former case, and agreement with wave shapes in the latter. Most authors mentioned, in passing, that the Earth's rotation was probably important to their studies but was nonetheless being ignored. In every case L_c was of the order of the width of the natural wave tank, and thus the wave structure would likely have been greatly modified by rotation. Based on the results of the present work, the effects are possibly even more dramatic, for not only should the actual Rossby radius, i.e. L_M, be half the value calculated on simple arguments, but also the wave curvature should be quite large. As an exercise, we have used the data of Hunkins & Fliegel (1973) to calculate the equilibrium effects to be expected. At their site 1, in the middle of the channel where the width is about 3.5 km they measured isotherm displacements of about 12 m on a mixed-layer depth of 15 m or so. The total fluid depth was some 165 m. Assuming a wave speed of 37 cm/s, i.e. in the middle of their reported range of values, we calculate L_c to be 3.8 km or $L_M = 1.9$ km (assuming such waves behave as the waves in our tank). We can now estimate the maximum wave amplitude on the eastern shore of the lake to be 30 m or a non-dimensional wave amplitude $A_w = 2$. Clearly nonlinear effects are very important in this case. Using our equation for wave angle we can in fact compute the wave shape, but, since no measurements are available to check it against, the exercise is best completed by only noting that the wave amplitude on the western shore would have been 4.7 m at site 1 and 2 m at site 2 (where the width is 5 km). Under these circumstances the maximum wave angles θ would have been 45° at site 1 and 50° at site 2. Such calculations imply that the maximum of wave amplitude on the western side would trail that on the eastern side by a distance of the order of the channel width (see figure 10), an effect which would have been readily observed. These authors also noted that the solitary wavetrains only appeared to propagate from south to north. While a large amplitude decrease is to be expected, due to substantial dissipation both while the wave propagated and due to interaction with the northern end of the lake, we suspect that a southward-travelling wave could still have been observed on the western side of the lake even if no disturbance was noted in the centre. Such a preference for south–north propagation has also been noted by Farmer (1978) in Babine Lake. In his case, however, there was a clear preference for generation in the south due to geographical and climatic constraints.

Of course a calculation such as that outlined above requires that the wave be in a state of geostrophic balance. The reported observations of Smith & Farmer (1977) suggest that the adjustment to geostropic balance may be quite slow if the initial waves produced by whatever generation mechanism, are two-dimensional. The waves observed in their study of generation by tidal flow over bottom topography appear, from their photograph, to be still quite two-dimensional a substantial distance (approximately 5 km) from the generation. However, the viewing angle is not very favourable for such observations, and may result in a false impression of the wave shape, as suggested by study of the more recent photographs discussed below. Based

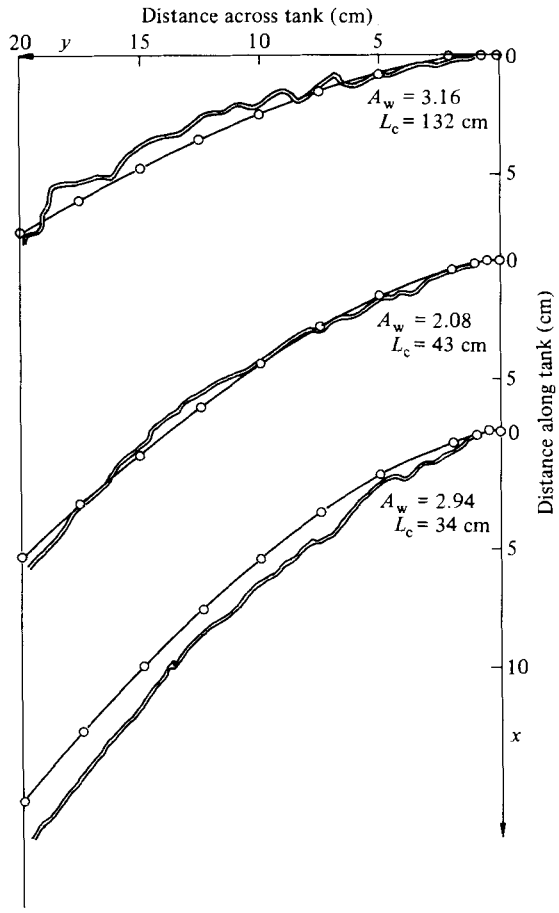

FIGURE 10. Calculated versus observed wave shape from plan view of the waves as in figures 2 and 3. The basis for this calculation is shown in figure 4 and explained in the text.

on potential-vorticity conservation within such large-amplitude waves, one can estimate a velocity in the direction of the wave crests as $2\Omega A\lambda$, where λ is the 'wavelength' of the solitary wave and A its dimensionless amplitude. The adjustment time can then be calculated as some fraction of the channel width divided by this velocity. For Knight Inlet, this turns out to be between 7 and 14 h, depending on the assumptions made, during which time the waves would have travelled between 12 and 24 km, while the wave decay time calculated from the results presented on figure 8 is 60–70 h. Such values appear to be typical of many limnological studies and suggest that indeed structures of the type observed in this study will be observed but only sufficiently far from the location of their generation if the latter is initially a two-dimensional process.

Dr David Farmer has kindly sent me three unpublished photographs of internal waves propagating westward on 16 August 1977 about 5–7 km from the location of generation in Knight Inlet and taken with the camera looking almost vertically downwards. The shape and location of the leading wave is reproduced in figure 11, and it has begun to show the curved shape that one might expect of a Kelvin wave. Any attempt to compare these shapes with those calculated using the method presented in §3 is frustrated by a lack of knowledge of the magnitude of the parameters,

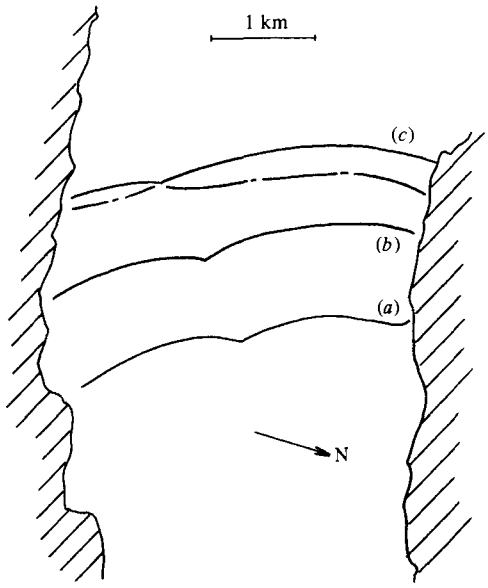

FIGURE 11. Sketch of the shape of the first of a group of internal wave propagation westward in Knight Inlet, transferred from photographs supplied by Dr D. M. Farmer of the Institute of Ocean Sciences, Sidney, B.C. The photographs were taken on 16 August 1977 at 16.11 h 30 s for (*a*), 16.27 h 20 s for (*b*) and 16.41 h 35 s for (*c*). In the latter case we have also drawn the second wave, chain-dotted, since it appears to interact with the first wave to the west. The curved shape into which this wave evolves is clearly related to the curved shapes we have observed in our experiments, although exact correspondence is probably confused by changes in wave speed due to changes in fluid depth, shoreline curvature and mean flow variations.

especially amplitudes, of these waves. Estimates based on other similar waves in Smith & Farmer (1977) suggest that those shown in figure 11 either have not yet evolved fully or are influenced by other effects that have not been considered up to now, e.g. the dependence of wave speed on fluid depth near shore, shoreline curvature (Clarke 1977) and shear in the mean flow, but the estimates are too crude to place reliance on these remarks.

In our present experimental arrangement, the initial generation mechanism is not two-dimensional, and it is in fact the adjustment of the initial collapse which controls the type of wave produced initially. This process is completed before the first wave is observed at the 80 cm station and so has no effect on our results. In future experiments we plan to study the adjustment process in detail and check the accuracy of the estimate made above.

One further example is contained in Baines (1980), where he developed a theory of the 'Southerly Buster', a coastal low-pressure front which appears to be strongly influenced by the presence of the Great Dividing Range in southeastern Australia. As a result of the interaction of a cold front with this mountain barrier a large-amplitude disturbance propagates rapidly northwards with the barrier to its left. A satellite photograph of the low-level cloud associated with such a front is reproduced in figure 12. Note particularly the curved shape of the front, a phenomenon which was commented on by Baines and for which he anticipated the explanation given in §3 of this paper!

Finally we note, in passing, a series of experiments by Suberville (1974), Chabert d'Hieres & Suberville (1976) and Kravtchenko & Suberville (1977) on forced internal

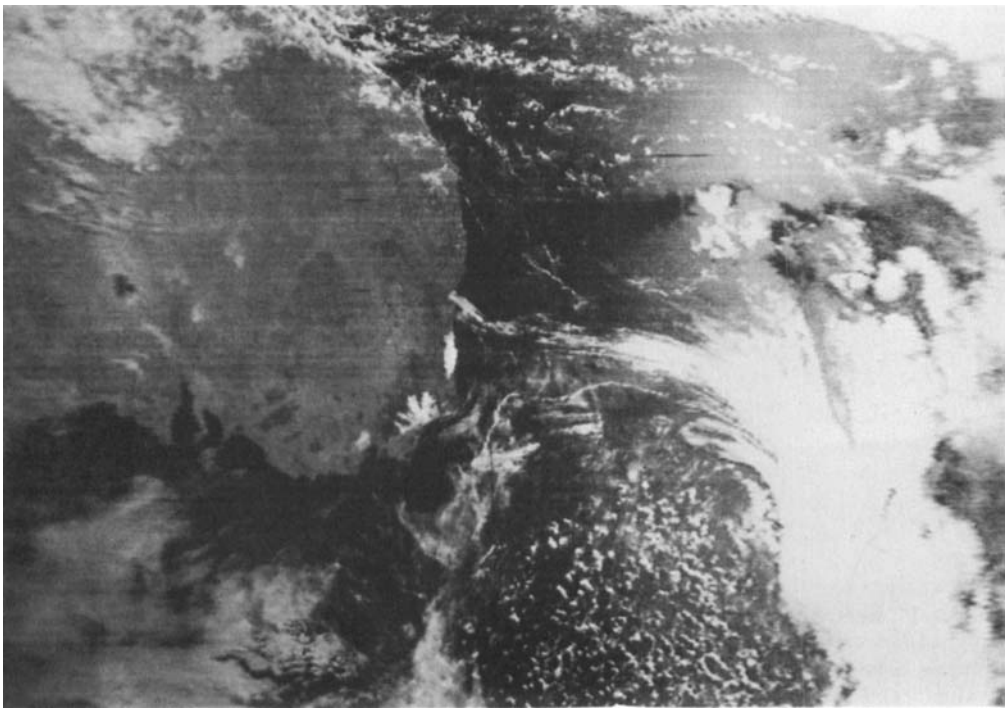

FIGURE 12. Satellite image of a Southerly Buster showing the backward curved shape as it propagates northwards (from Baines 1980).

waves in a rotating, rectangular container, i.e. a rotating version of Thorpe's (1974) experiment, in which many of the features of interface distortion described qualitatively by Mortimer (1955) are reproduced. Suberville (G. Chabert d'Hieres, private communication) also photographed solitary internal Kelvin waves in the same apparatus for a demonstration film, but these were not analysed in any detail.

The majority of the experiments reported here were performed by Frances Teng of the Polytechnic School, Pasadena. The quality of the results owe much to her care, thoughtfulness and ingenuity. The results were analysed and prepared for publication while on leave at the University of Karlsruhe as a U.S. Senior Scientist Awardee (1981–82) of the von Humboldt Foundation. I am deeply grateful to Professor Franz Durst for nominating me for this award and for placing the facilities of his group at my disposal during my stay. I am most grateful to Dr K. Heikes for the development and programming that led to the numerical calculations of figure 7, which were one of the keys to the understanding of the role played by inertial waves in the decay of the internal Kelvin waves. The apparatus was skilfully constructed by Casey DeVries, while Jacquette Givens patiently typed the many revisions that were required as new information became available. The work was supported by the Office of Naval Research through both the Fluid Dynamics and Oceanography Divisions under Contract no. N0001482K0084 to the University of Southern California.

REFERENCES

AMEN, R. and MAXWORTHY, T. 1980 The gravitational collapse of a mixed region into a linearly stratified fluid. *J. Fluid Mech.* **96**, 65.

ANH, N. N. & GILL, A. E. 1981 The generation of coastal lows by synoptic scale wave. *Q. J. R. Met. Soc.* **107**, 521.

BAINES, P. G. 1980 The dynamics of the Southerly Buster. *Austral. Met. Mag.* **28**, 175.

BANNON, P. R. 1981 Synoptic scale forcing of coastal lows: forced double Kelvin waves in the atmosphere. *Q. J. R. Met. Soc.* **107**, 313.

BENJAMIN, T. B. 1967 Internal waves of permanent form in fluids of great depth. *J. Fluid Mech.* **29**, 559.

BRITTER, R. E. & SIMPSON, J. E. 1978 Experiments on the dynamics of a gravity current head. *J. Fluid Mech.* **88**, 223.

BRITTER, R. E. & SIMPSON, J. E. 1981 A note on the structure of the head of a intrusive gravity current. *J. Fluid Mech.* **112**, 459.

CHABERT D'HIERES, G. & SUBERVILLE, J. L. 1976 A theoretical and experimental study of internal waves in a rotating-stratified medium. In *Proc. 14th Congress IUTAM, Delft*, vol. 2.

CLARKE, A. J. 1977 Wind-forced linear and non-linear Kelvin waves along an irregular coast. *J. Fluid Mech.* **83**, 337.

FARMER, D. M. 1978 Observations of long nonlinear internal waves in a lake. *J. Phys. Oceanogr.* **8**, 63.

FARMER, D. M. & SMITH, J. D. 1980 Tidal interaction of stratified flow with a sill in Knight Inlet. *Deep-Sea Res.* **27A**, 239.

FAUST, K. M. 1981 Intrusion of a density front into a stratified environment. *Report III, Univ. Karlsruhe, Inst. F. Wasserbau III.*

GAUNTLETT, D. J. 1981 The numerical simulation of intense frontal discontinuities over South Eastern Australia. In *Proc. I.A.M.A.P. Nowcasting Symp., Hamburg.*

HAMBLIN, P. F. 1978 Internal Kelvin waves in a fjord lake. *J. Geophys. Res.* **83**, 2409.

HEIKES, K. & MAXWORTHY, T. 1982 Observations of inertial waves in a homogeneous, rotating fluid. *J. Fluid Mech.* **125**, 319.

HUNKINS, D. & FLIEGEL, M. 1973 Internal undular surges in Seneca Lake: a natural occurrence of solitons. *J. Geophys. Res.* **78**, 539.

JOSEPH, R. I. 1977 Solitary waves in a finite depth fluid. *J. Phys.* A: *Math. (Gen.)* **10**, L255.

KRAVTCHENKO, J. & SUBERVILLE, J.-L. 1977 Étude théorique des ondes internes dans les eaux d'un basin en rotation. *Annales Hydrographiques 5ème série* **5**, fascl. no. 476, 95–116.

MASON, P. J. & SYKES, R. J. 1983 A numerical study of rapidly rotating flow over surface-mounted obstacles. Submitted to *J. Fluid Mech.*

MAXWORTHY, T. 1980 On the formation of nonlinear, internal waves from the gravitational collapse of mixed regions in two and three dimensions. *J. Fluid Mech.* **96**, 47.

MORTIMER, C. H. 1955 Some effects of the Earth's rotation on water movements in stratified lakes. *Proc. Intl Assoc. Appl. Limnol.* **12**, 66.

PEDLOSKY, J. 1979 *Geophysical Fluid Dynamics.* Springer.

SMITH, J. D. & FARMER, D. M. 1977 Non-linear internal waves and hydraulic jumps in a fjord. In *Geofluiddynamic Wave Mathematics*, pp. A2–53. University of Washington, Seattle.

STERN, M. E., WHITEHEAD, J. A. & HUA, B. L. 1982 The intrusion of a density current along the coast of a rotating fluid. *J. Fluid Mech.* **123**, 237.

SUBERVILLE, J.-L. 1974 Ondes internes en fluide tournant. Contribution théorique et expérimentale. Thèse, L'Université Scientifique et Médicale de Grenoble.

THORPE, S. A. 1971 Asymmetry of the internal surge in Loch Ness. *Nature* **231**, 306.

THORPE, S. A. 1974 Near-resonant forcing in a shallow two-layer fluid: a model for the internal surge in Loch Ness? *J. Fluid Mech.* **63**, 509.

THORPE, S. A., HALL, A. & CROFTS, I. 1972 The internal surge in Loch Ness. *Nature* **237**, 96.

WEIDMAN, P. D. & MAXWORTHY, T. 1978 Experiments on strong interactions between solitary waves. *J. Fluid Mech.* **85**, 417.